Journal of Chromatography, 559 (1991) 27–42
Elsevier Science Publishers B.V., Amsterdam

CHROM. 23 417

Temperature elevations of the sample zone in free solution capillary electrophoresis under stacking conditions

ANDERS VINTHER*
Department of Fermentation Physiology, Novo Nordisk, Lagergårdsvej 2, DK-2820 Gentofte (Denmark)
and
HENRIK SØEBERG
Department of Chemical Engineering, Technical University of Denmark, Building 229, DK-2800 Lyngby (Denmark)

ABSTRACT

The combination of a low specific conductivity ratio of sample solution to surrounding running buffer (under stacking conditions) and high applied potentials can result in high power inductions and high temperatures of the sample zone. Eventually boiling occurs. Calculations of the sample zone and running buffer temperatures are based on changes in viscosity, relative permittivity, zeta potential and specific conductivity of the buffer solutions as a function of temperature. The temperature gradients across the capillary inner radius, the glass wall, the polyimide coating and the "thermo layer" from the capillary outer coating to the surroundings are estimated. Heat-transfer coefficients for liquid- and air-cooled capillaries were obtained.

INTRODUCTION

One of the characteristics of high-performance capillary electrophoresis (HPCE) [1,2] is the high peak efficiences due to the plug-like so-called electroosmotic flow profile [3–5]. With optimized separation conditions, theoretical plate numbers of the order of 10^5–10^6 are obtainable on a routine basis. There are, however, several factors that can cause excessive band broadening and loss of resolution [5–16]. One of these factors is Joule heating.

Most often high voltages are applied in HPCE with typical average field strengths in the range 50–1000 V cm^{-1}. Power is assumed to be uniformly induced across the capillary cross-sectional area, but only removed at the capillary wall (and at the capillary ends). This results in a parabolic temperature profile in the liquid inside the capillary tube with the maximum temperature being at the axis. The combination of highly conductive buffers and/or high field strengths results in high power inductions and the Joule heat produced causes the analyte zone to be excessively dispersed.

The general approach when minimizing dispersion due to Joule heating is to

0021-9673/91/$03.50

remove the heat effectively by the use of capillaries with a high surface-to-volume ratio (narrow-bore tubes) and a thermostated forced convection. Several workers have described how effectively peak efficiencies can be improved by lowering the capillary radius [9,10,13–19]. The drawback of lowering the capillary radius is a decreased path length for UV absorbance detection. Knox [19] and Grushka and co-workers [17,18] showed that most of the temperature gradient from the capillary tube axis to the surroundings was in the "thermo layer" from the capillary outer coating to the surroundings. Nelson *et al.* [20] compared different means of heat removal and found the order of effectiveness to be Peltier device > fan cooling > natural convection.

Estimations of, among others, the sample plug and running buffer temperatures as a function of radial position under various stacking conditions are reported here. A knowledge of the sample zone and running buffer temperatures during capillary electrophoresis analysis is crucial (a) when heat-labile analytes are employed and (b) when describing the dispersion processes by mathematical modelling. This is especially true when stacking conditions prevail.

Sample stacking (concentration of the analyte zone) is the process that occurs when a voltage is applied along a capillary tube containing a sample plug with a lower specific conductivity than that of the surrounding running buffer. As the electric field strength is inversely proportional to the specific conductivity of the liquid, the field strength is higher along the sample plug compared with the running buffer. In this way the electrophoretic velocity, which is proportional to the field strength, increases and the ionic analyte zone is narrowed. This "reversed dispersion" is termed sample stacking.

The HPCE experiments were performed in the free solution capillary electrophoresis [21] (FSCE) mode. When FSCE analysis is performed under stacking conditions with a large difference between the sample plug and running buffer specific conductivities, high temperature elevations of the analyte zone can result when applying a voltage.

All the experiments were carried out with biosynthetic human growth hormone (B-hGH) as the analyte. B-hGH is a 22 125 relative molecular mass protein consisting of 191 amino acids with an isoelectric point of *ca.* pH 5. Analysis was performed at pH 8.0, where B-hGH is a convenient choice of analyte as it has a suitable net mobility and is repelled from the capillary surface.

EXPERIMENTAL

Materials

Tricine {N-[tris(hydroxymethyl)methyl]glycine} and sodium chloride were purchased from Fluka (Buchs, Switzerland) and B-hGH from Novo Nordisk (Gentofte, Denmark). Fused-silica capillaries were obtained from Polymicro Technologies (Phoenix, AZ, USA). Peak areas were integrated on a Shimadzu C-R5A integrator (Kyoto, Japan).

Methods

Analysis was performed on an Applied Biosystems Model 270A analytical capillary electrophoresis system. The fused-silica capillaries had an I.D. of 50 μm, an O.D. of 192 μm, a total length of 100 cm and a length of 75 cm to the detector (effective

length). From the introduction end to the detector the capillaries were surrounded by a thermostated air-bath operated at 27°C. The electroosmotic flow was determined by measuring the retention time of the peak of neutral species.

Unless stated otherwise, the experimental conditions were as follows. Samples were introduced for 3 s by applying a 16.8-kPa vacuum at the detector end of the capillary. A 10 m*M* tricine (pH 8.0)–25 m*M* NaCl running buffer (specific conductivity at 21°C, $\kappa_{21°C} = 2.75$ mS cm^{-1}) was used. The applied potential was changed from 5 to 30 kV in steps of 5 kV. Detection was performed at 200 nm. Two series of experiments were performed: one with stacking and the other with non-stacking conditions. During the stacking runs B-hGH was diluted with distilled water to 0.1 mg ml^{-1} ($\kappa_{21°C} = 0.17$ mS cm^{-1}), whereas under non-stacking conditions B-hGH as diluted to the same concentration with running buffer ($\kappa_{21°C} = 2.75$ mS cm^{-1}).

THEORY

From experiments the electroosmotic mobility, μ_{EO}, can be measured as

$$\mu_{EO} = \frac{v_{EO}}{E} = \frac{L_d L_c}{t_{EO} U} \tag{1}$$

where v_{EO} is the electroosmotic velocity, E is the field strength, U is the applied voltage, t_{EO} is the retention time of the neutral species and L_d and L_c are the effective and total length of the capillary, respectively.

Fig. 1 shows the measured μ_{EO} values from the non-stacking experimental runs.

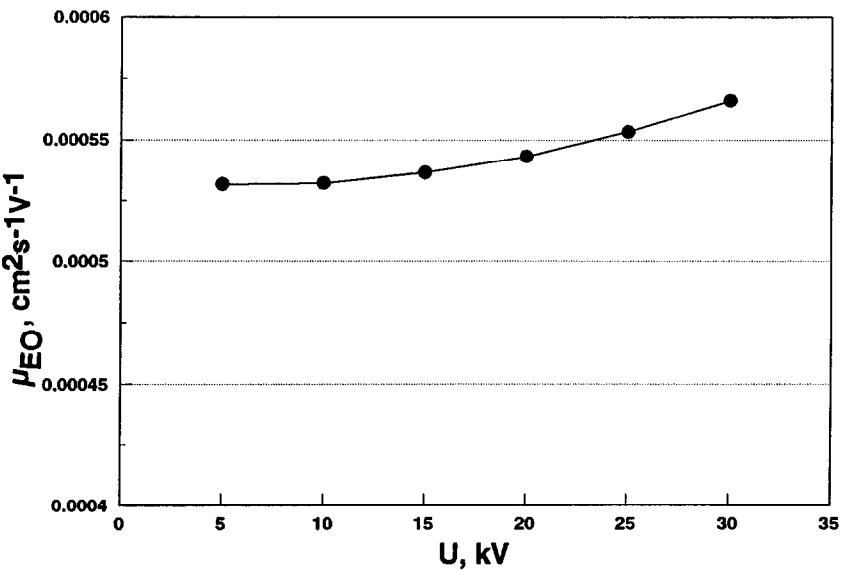

Fig. 1. Experimentally obtained electroosmotic mobility (μ_{EO}, cm^2 V^{-1}s^{-1}) *vs.* the applied potential (U, kV) in the non-stacking experiments. μ_{EO} was calculated by eqn. 1 after measuring the retention time of the peak of neutral species. The running buffer was 10 m*M* tricine (pH 8.0) containing 25 m*M* NaCl. The thermostated air-bath temperature was 27°C and the total capillary length was 100 cm. Other conditions as under Experimental.

As the only parameter changed during the experiment is the applied potential, the increase in μ_{EO} with increasing U must be due to an increased temperature of the running buffer.

In order to estimate the elevated temperature, instead of eqn. 1 μ_{EO} can be written as a function of one constant [the permittivity of vacuum ($\varepsilon_0 = 8.854 \cdot 10^{-14}$ C^2 cm^{-1} J^{-1})] and three temperature-dependent parameters {the relative permittivity (ε_r), the zeta potential [22,23] (ζ) and the viscosity (η)}:

$$\mu_{EO} = \frac{\varepsilon_0 \varepsilon_r \zeta}{\eta} \tag{2}$$

In order to estimate the average temperature change during analysis, a knowledge of how ε_r, ζ and η vary with temperature is crucial. In the HPCE literature most often it is assumed that the variations of ε_r and ζ can be neglected compared with the variations of η with temperature [18,24]. We do, however, use all three variables as functions of the temperature.

Calculation of ε_r

According to ref. 25, the relative permittivity change is related to the temperature change, dT, by

$$-\frac{\mathrm{d}\log_{10}\varepsilon_r}{\mathrm{d}T} = 0.00200 \tag{3}$$

Integrating ε_r from $\varepsilon_r(298\ \mathrm{K}) = 78.54$ to $\varepsilon_r(T)$ yields

$$\varepsilon_r = 309.78 \exp(-0.004605T) = c_{\varepsilon 1} \exp(-c_{\varepsilon 2} T) \tag{4}$$

Calculation of η

In the temperature range 20–100°C the viscosity of water (cP) is related to the temperature (T, °C) by

$$\log\left(\frac{\eta}{\eta_{20}}\right) = \frac{1.3272(20 - T) - 0.001053(T - 20)^2}{T + 105} \tag{5}$$

where η_{20} is the viscosity at 20°C [25]. As an approximation, eqn. 5 is simplified to (T in K)

$$\eta = \frac{1}{800} \exp\left(\frac{1958}{T}\right) = c_{\eta 1} \exp\left(\frac{c_{\eta 2}}{T}\right) \tag{6}$$

Calculation of ζ

The zeta potential is considered to be proportional to temperature [22]:

$$\zeta = c_\zeta T \tag{7}$$

where T is in K and $c_\zeta = 4(k_{Bltz}/ze)$ mV K^{-1}, k_{Bltz}, z and e being the Boltzmann constant ($1.381 \cdot 10^{-23}$ J K^{-1}), the number of charges and the elementary charge ($1.602 \cdot 10^{-19}$ C), respectively.

Calculation of μ_{EO}

When the same running buffer is used throughout a series of experiments, where U is the only parameter changed from run to run, the mean temperature, T, during analysis can be calculated by the use of a reference μ_{EO} value where the temperature is known (T_{ref}):

$$\mu_{EO} \cdot \frac{\eta}{\varepsilon_0 \varepsilon_r \zeta} = \mu_{EO,ref} \cdot \frac{\eta_{ref}}{\varepsilon_0 \varepsilon_{r,ref} \zeta_{ref}} \tag{8}$$

Combining eqns. 4 and 6–8 and solving for μ_{EO} results in

$$\mu_{EO} = \mu_{EO,ref} \exp\left[c_{\eta 2}\left(\frac{1}{T_{ref}} - \frac{1}{T}\right) + c_{\varepsilon 2}(T_{ref} - T) \right] \frac{T}{T_{ref}} \tag{9}$$

Once the temperature T has been estimated, the viscosity and relative permittivity are calculated by the use of eqns. 4 and 6. The zeta potential is estimated relative to that at the reference temperature (eqn. 7), which in turn is estimated by rearranging eqn. 2:

$$\zeta_{ref} = \mu_{EO,ref} \cdot \frac{\eta_{ref}}{\varepsilon_0 \varepsilon_{r,ref}} \tag{10}$$

Power vs. temperature elevation

A linear relationship between dT and P (P is the power induced = UI, where I is the current) is assumed:

$$P = a\mathrm{d}T + b \approx a\mathrm{d}T \tag{11}$$

where a and b are constants. This is a simplification of reality, but the presumption is acceptable in the experiments (see Results and Discussion) as it does not induce serious errors in the temperature model. The actual dT–P curve deviates slightly from linearity at high dT values. Hence the dT values are not as large as would be expected from eqn. 11.

Radiation of energy

One of the factors that can make the dT–P curve deviate from linearity is the net radiation of energy per unit area from the capillary to the surroundings. In accordance with the Stefan–Boltzmann law, the radiation of energy is

$$Q = Q_{capillary} - Q_{surroundings} = \varepsilon_{capillary}\sigma_{Stf}T^4_{capillary} - \varepsilon_{surroundings}\sigma_{Stf}T^4_{surroundings} \tag{12}$$

where σ_{Stf} is the Stefan–Boltzmann constant ($5.67 \cdot 10^{-8}$ W m^{-2} K^{-4}) and ε_x is the

dimensionless emissivity constant, which is 1 for black bodies and <1 for all other bodies. If $T_{\text{capillary}} = 373.15$ K (100°C) and the 192 μm O.D. capillary is assumed to be a black body, the radiation of power from the 100-cm capillary would be 0.66 W, thus decreasing dT by less than 3°C (eqn. 11; see Results and Discussion). This must be compared with a temperature increase of *ca.* 73°C due to Joule heating of the capillary. As the actual net radiation from the capillary is even lower than 0.66 W at 100°C (emissivity constant <1, and subtraction of the radiation from the surroundings), the radiation of energy is neglected in the model.

Non-uniform electric field

When the conductivity of the sample zone differs from that of the running buffer, so do the field strength and the temperature during analysis [5,26]. In order to estimate the temperature of the buffer and sample zone, a few calculations have to be made.

The power which is induced in the capillary is separated into (a) power induced in the running buffer, P_B:

$$P_B = I^2 R_B = I^2 \cdot \frac{L_B}{A\kappa_B} = I^2 \cdot \frac{L_c - L_0}{A\kappa_B} \tag{13}$$

and (b) power induced in the sample zone, P_S:

$$P_S = I^2 R_S = I^2 \cdot \frac{L_0}{A\kappa_S} \tag{14}$$

Hence,

$$P = P_B + P_S = \frac{I^2}{A}\left(\frac{L_c - L_0}{\kappa_B} + \frac{L_0}{\kappa_S}\right) \tag{15}$$

Subscripts B and S denote buffer and sample solution, respectively; A is the cross-sectional area, R is the resistance, κ is the specific conductivity and L_B and L_0 are the length of the buffer and the originally introduced sample zone, respectively. Combining eqns. 13–15 and solving eqn. 15 with respect to P_B and P_S results in

$$P_B = \frac{P}{1 + X} \tag{16}$$

$$X \equiv \frac{\kappa_B L_0}{\kappa_S (L_c - L_0)} \tag{17}$$

and

$$P_S = P_B X = \frac{P}{\frac{1}{X} + 1} \tag{18}$$

Now the temperature elevations of the running buffer, dT_B, and of the sample zone, dT_S, can be estimated with the use of eqn. 11:

$$dT_B = \frac{P_B L_c}{a(L_c - L_0)} = \frac{PL_c}{a(1 + X)(L_c - L_0)} \tag{19}$$

$$dT_S = \frac{P_S L_c}{aL_0} = \frac{PL_c}{a\left(\frac{1}{X} + 1\right)L_0} \tag{20}$$

Specific conductivity vs. temperature

As the running buffer and sample zone experience different temperature elevations under stacking conditions, it remains to find the specific conductivity as a function of the temperature. From experiments, identical and linear conductivity index (CI) *vs.* T (T in °C) curves were obtained (see Results and Discussion), where CI is defined as

$$CI = 100 \cdot \frac{\kappa_T}{\kappa_{21°C}} = c_{\kappa 1} + c_{\kappa 2} T \tag{21}$$

Eqns. 16–21 are solved iteratively in order to estimate the specific conductivities and temperatures of the running buffer and sample zone during each run in the stacking and non-stacking runs.

Temperature gradient as a function of radial position

Fig. 2 is a schematic diagram of a capillary tube. The total temperature

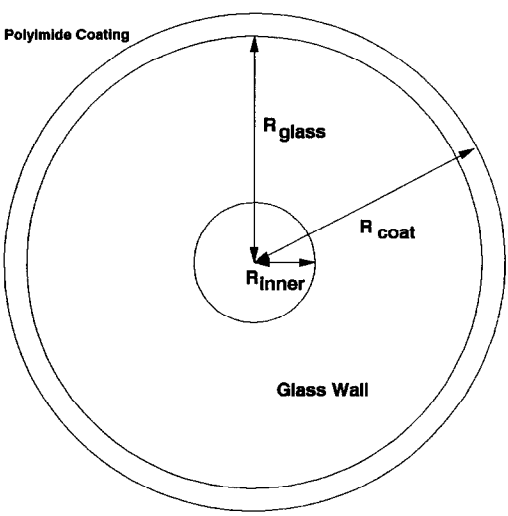

Fig. 2. Schematic diagram of a capillary tube. R_{inner} = distance from capillary axis to inner radius; R_{glass} = distance from capillary axis to the glass wall outer radius; R_{coat} = distance from capillary axis to outer radius.

difference between the centre of the capillary tube and the air-bath is made up of four contributions:

$$dT = dT_{inner} + dT_{glass} + dT_{coat} + dT_{surr} \tag{22}$$

where dT_{inner}, dT_{glass}, dT_{coat} and dT_{surr} are the temperature gradients from the centre of the tube to the capillary inner radius, across the glass wall, across the polyimide coating and from the capillary outer jacket to the surroundings, respectively.

Owing to the temperature-dependent electroosmotic and electrophoretic mobilities, a knowledge of the temperature difference from the centre of the tube to the fused-silica glass wall, dT_{inner}, is of special interest when considering dispersion. By use of eqn. 9 the electroosmotic mobility is calculated to increase by 2–3% per °C in the range 20–100°C.

The temperature difference from the centre of the tube to the capillary inner radius, R_{inner}, is found by solving the heat conduction equation [27]

$$\frac{1}{r}\left(\frac{d}{dr}\right)\left[rk_w\pi R_{inner}^2 L_c \cdot \frac{dT_{inner}(r)}{dr}\right] = -P \tag{23}$$

where r is the variable radius and k_w is the thermal conductivity of the buffer. Integrating eqn. 23 with the appropriate boundary conditions yields

$$dT_{inner} = P \cdot \frac{1}{4\pi k_w L_c} = c_{inner}P \tag{24}$$

at the glass wall where $r = R_{inner}$.

dT_{glass} and dT_{coat} are calculated by solving equations similar to eqn. 23 and integrating from R_{inner} to R_{glass} (radius from the tube axis to the polyimide coating) and from R_{glass} to R_{coat} (radius from the tube axis to the outside of the polyimide coating), respectively. The solutions are

$$dT_{glass} = \frac{\ln\left(\frac{R_{glass}}{R_{inner}}\right)}{2\pi k_{glass} L_c} \cdot P = c_{glass}P \tag{25}$$

and

$$dT_{coat} = \frac{\ln\left(\frac{R_{coat}}{R_{glass}}\right)}{2\pi k_{coat} L_c} \cdot P = c_{coat}P \tag{26}$$

The temperature gradient across the air film from the capillary outer wall to the thermostated air-bath, dT_{surr}, is calculated by subtraction of the three other dT_x terms from the total temperature difference, dT, which was found by eqn. 9. Hence,

$$dT_{surr} = \frac{P}{a} - c_{inner}P - c_{glass}P - c_{coat}P = c_{surr}P \tag{27}$$

The heat-transfer coefficient, h, indicates the effectiveness of the heat removal from the air film on the capillary polyimide coating to the surroundings. h is estimated by combining eqn. 27 with Newton's law of cooling [27]:

$$P = hA\mathrm{d}T_{\mathrm{surr}} \tag{28}$$

thus yielding

$$h = \frac{1}{c_{\mathrm{surr}}A} \tag{29}$$

RESULTS AND DISCUSSION

Estimation of buffer temperature

As the slope of the experimentally obtained μ_{EO} curve from 5 to 10 kV in Fig. 1 is approximately zero, it is reasonable to assume that there is no increase of the buffer temperature relative to the thermostated air-bath surrounding the capillary. Hence, inserting $T_{\mathrm{ref}} = 300$ K (27°C), $\mu_{\mathrm{EO,ref}} = \mu_{\mathrm{EO}}$ (300 K, 5 kV) and the measured μ_{EO} values in eqn. 9 and solving iteratively for T, the temperatures of the running buffer are estimated in the remainder of the runs (10–30 kV).

Fig. 3 shows the calculated temperature elevations. The η, ε_{r} and ζ values (calculated by eqns. 4, 6 and 10) are depicted in Fig. 4 relative to the values at 27°C (300 K), and Table I contains the absolute values. The relative changes of ε_{r} and ζ as a function of U approximately cancel each other out.

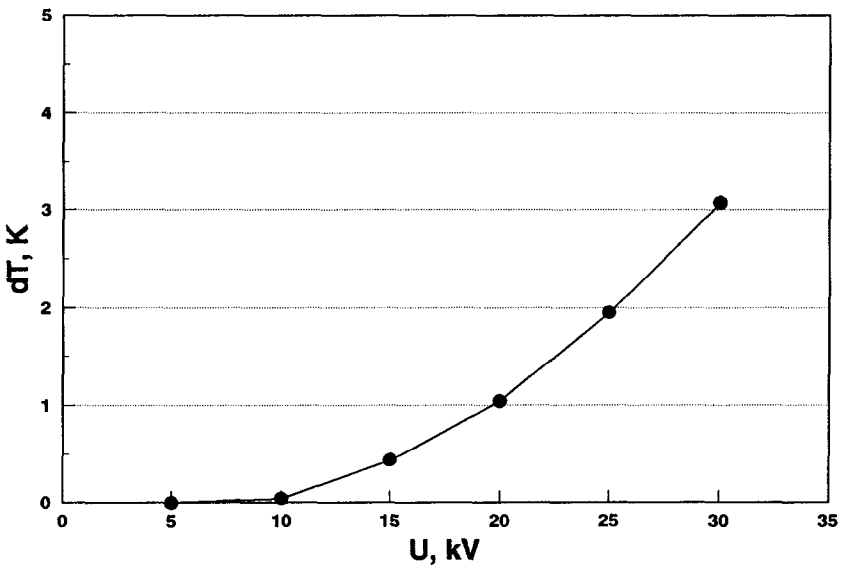

Fig. 3. Calculated temperature elevations (dT, K) of the running buffer *vs.* the applied potential (U, kV) in the non-stacking experiments. The dT values are found by inserting the measured μ_{EO} values in eqn. 9 and solving iteratively with respect to T. Experimental conditions as in Fig. 1.

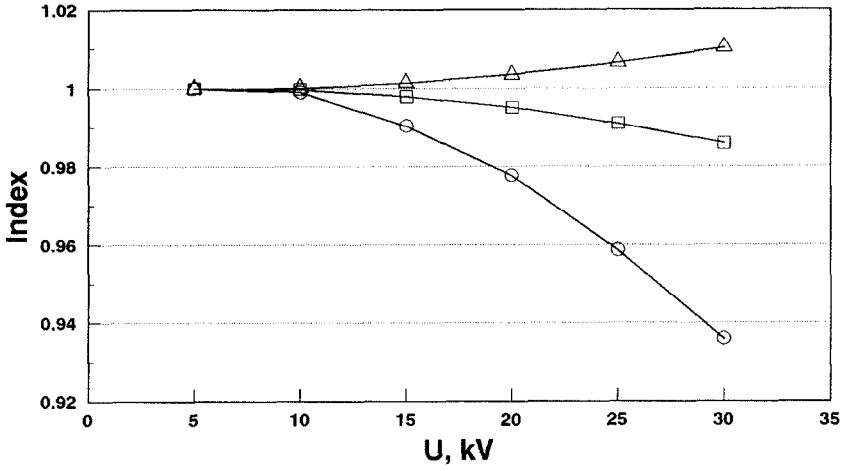

Fig. 4. Calculated (○) relative viscosity (η), (□) relative permittivity (ε_r) and (△) zeta potential (ζ) *vs.* applied potential (U, kV). The η, ε_r and ζ values are shown relative to the values in the 5-kV run. Table I summarizes the absolute values. Experimental conditions as in Fig. 1.

Power vs. temperature elevation

A plot of the measured average power, $P = UI$, *vs.* the estimated temperature changes, dT, results in Fig. 5. As assumed in eqn. 11, omitting the lowest x-value point on the curve a linear dT *vs.* P relationship is observed with slope $a = 0.207$ W K^{-1} and intercept with the ordinate $b = 0.073$ W.

The reason for the non-zero intercept of the power curve and the ordinate, is explained as being due to the $dT = 0$ assumption in the 5-kV experiment. For simplicity b is neglected when estimating dT from the measured P values (error 0.35 K).

Specific conductivity vs. buffer temperature

In order to relate the specific conductivity to the temperature of the running buffers, the specific conductivities of three 10 mM tricine running buffers (pH 8.0) containing (a) 0 mM NaCl ($\kappa_{21°C} = 0.22$ mS cm^{-1}), (b) 25 mM NaCl ($\kappa_{21°C} = 2.75$ mS cm^{-1}) or (c) 50 mM NaCl ($\kappa_{21°C} = 4.96$ mS cm^{-1}) were measured in the temperature range 21–93°C by heating the buffer in a stirred beaker. In Fig. 6 the resultant conductivity index (CI) values are plotted *vs.* the measured temperatures. In

TABLE I

ABSOLUTE VALUES OF THE VISCOSITY (η), RELATIVE PERMITTIVITY (ε_r) AND ZETA POTENTIAL (ζ) FROM EXPERIMENTS AS A FUNCTION OF THE APPLIED POTENTIAL (E_{app}) AND THE TEMPERATURE ELEVATION (dT) IN THE NON-STACKING RUNS

U	dT (K)	η (cP)	ε_r	ζ (mV)
5	0.00	0.851	77.82	65.73
10	0.04	0.850	77.80	65.74
15	0.44	0.843	77.66	65.83
20	1.04	0.832	77.45	65.96
25	1.95	0.816	77.12	66.16
30	3.08	0.797	76.73	66.41

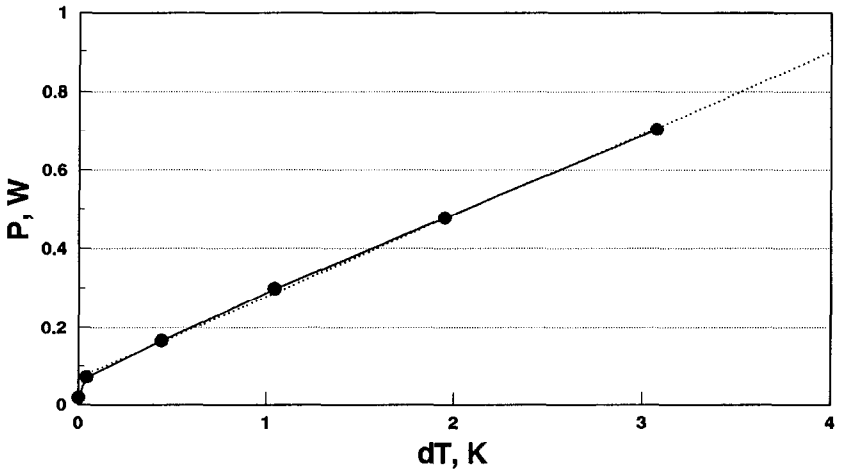

Fig. 5. Measured power inductions ($P = UI$, W) *vs.* the calculated temperature elevations (dT, K) in the non-stacking experiment. Omitting the lowest x-value point, linear regression yields $P = 0.207\,dT + 0.073$. The correlation factor is 0.9992. See text and Experimental for details. ●—● = Experiments; dotted line = linear regression.

accordance with eqn. 21, linearity is observed. The constants in eqn. 21 were found to be $c_{\kappa 1} = 38.67$ and $c_{\kappa 2} = 2.62°C^{-1}$ by linear regression on all data points.

Sample zone temperature, stacking vs. non-stacking conditions

Solving eqns. 16–21 iteratively with the appropriate experimental values yields the specific conductivities and temperatures of the running buffer and sample zone during each run under stacking and non-stacking conditions. The results are shown in

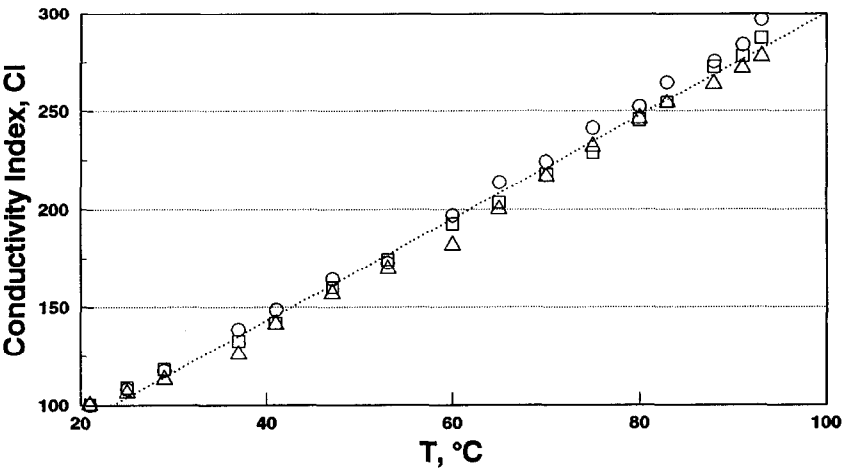

Fig. 6. Conductivity index ($CI = 100\kappa_T/\kappa_{21°C}$) *vs.* the temperature (T, °C) for three 10 mM tricine buffers (pH 8.0) containing (○) 0, (□) 25 or (△) 50 mM NaCl. The buffer was heated in a stirred beaker and the specific conductivity measured in the range 21–93°C. A linear CI–T relationship is observed. Linear regression (dotted line) on all data points gave a correlation factor equal to 0.9961.

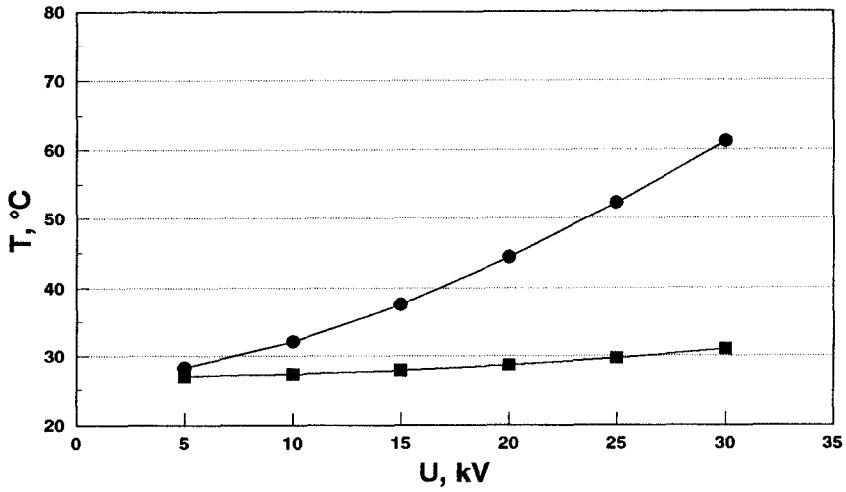

Fig. 7. Estimated sample zone temperature (T, °C) *vs.* the applied potential (U, kV) in the (●) stacking and (■) non-stacking runs. The sample zone experiences higher temperatures when diluted with distilled water (stacking) compared with dilution with running buffer (non-stacking).

Fig. 7 with respect to sample zone temperature. When the analyte is diluted with distilled water, the temperature elevation at any U is higher than that experienced when diluting the analyte with the running buffer. The reason for the higher temperature of the sample zone during stacking conditions is due to the specific conductivity difference between the running buffer and the sample solution, thus resulting in different field strengths.

This is further elaborated in Fig. 8. Three 10 mM tricine buffers (pH 8.0) containing either 0, 25 or 50 mM NaCl were used in three experimental series. The B-hGH analyte was diluted to 0.1 mg ml^{-1} with distilled water ($\kappa_{21°C}$ = 0.17 mS cm^{-1}). As the specific conductivity of the sample was lower than that of any of the three running buffers, stacking conditions prevailed in all three experimental series. The purpose of the three experiments was to show the effect of different "stacking powers" (κ_B/κ_S) on the sample zone temperature elevations.

The highest temperature elevation of the buffer zone was experienced in the 30-kV run with the 50 mM NaCl tricine buffer [T_B (50 mM) *ca.* 6°C], where the induced power was *ca.* 1.4 W. However, when the specific conductivity ratio κ_B/κ_S and the specific conductivity of the buffer solution, κ_B, are both high, the sample zone reaches very high temperatures at high applied potentials. At 30 kV with the 50 mM NaCl tricine buffer as running buffer the sample zone is close to the boiling point [T_S (50 mM)] according to the estimations.

When the temperature of the sample zone increases more than the temperature elevation of the running buffer (owing to the different field strengths), the specific conductivity ratio decreases compared with the ratio which is experienced when the two solutions have the same temperature. This change is taken into consideration in eqn. 21 and shown in Fig. 9 for the three experimental series with running buffers of different NaCl concentration.

One must consider the temperature of the analyte zone when the analysis is

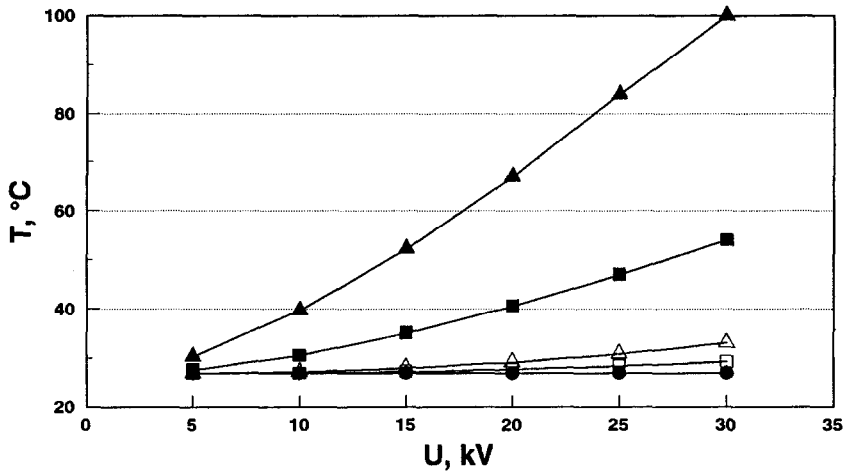

Fig. 8. Estimated temperatures of (open symbols) the running buffer (T_B, °C) and (closed symbols) the sample zone (T_S, °C) *vs.* the applied potential (U, kV). The sample was B-hGH diluted to 0.1 mg ml^{-1} with distilled water ($\kappa_{21°C}$ = 0.17 mS cm^{-1}). Sample was introduced for 1.0 s by means of a 16.8-kPa vacuum. All the runs were performed under stacking conditions. Three experimental series were carried out in 10 m*M* tricine buffers (pH 8.0) containing (○, ●) 0 m*M* NaCl ($\kappa_{21°C}$ = 0.22 mS cm^{-1}), (□, ■) 25 m*M* NaCl ($\kappa_{21°C}$ = 2.75 mS cm^{-1}) or (△, ▲) 50 m*M* NaCl ($\kappa_{21°C}$ = 4.96 mS cm^{-1}). Other conditions as under Experimental.

performed using stacking conditions. As long as the analyte zone is still in the original sample zone, it will experience an elevatad temperature compared with that of the running buffer. The fact that the temperature elevations can even become so dramatic that boiling of the sample zone is possible under certain experimental conditions is

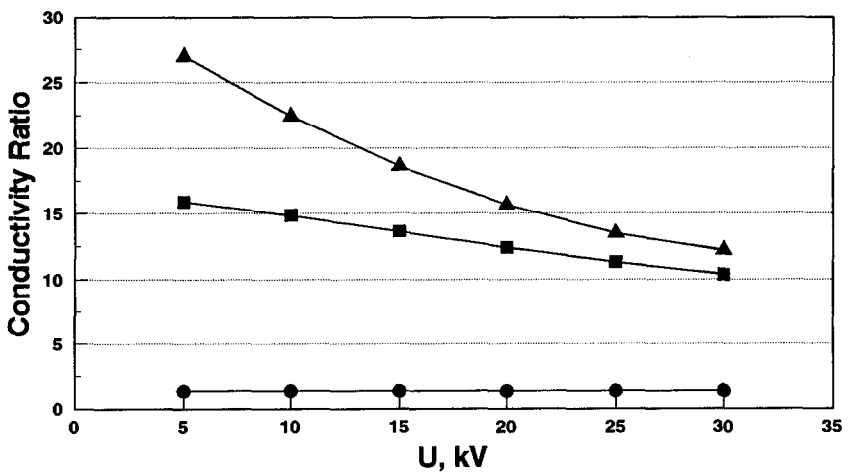

Fig. 9. Specific conductivity ratio (κ_B/κ_S) *vs.* the applied potential (U, kV) in the three experimental series, where the running buffer contained (●) 0, (■) 25 or (▲) 50 m*M* NaCl. Experimental conditions as in Fig. 8. As the difference in temperature between the sample zone and the running buffer increases with higher U, the specific conductivity ratio decreases in accordance with eqn. 21.

interesting. Most important, however, is that knowledge of the temperature elevation can be crucial when the analyte is heat-labile. In that event high temperatures resulting in degradation of the analyte could be misinterpreted as, *e.g.*, impurities in the original sample.

Temperature calculations based on Ohm's law

As an alternative to the electroosmotic mobility-based temperature estimations, which are used in this model, the temperature elevations could be based on eqn. 21 and Ohm's law. The values obtained in this way varies by less than 6% from the already estimated values. Owing to the different specific conductivities along and across the capillary tube, and the current contributions from ions making up the electroosmotic flow, all the temperature calculations shown here are, however, based on changes in the electroosmotic mobilities.

Temperature gradient as a function of radial position

Inserting $R_{inner} = 25$ μm, $R_{glass} = 90$ μm, $R_{coat} = 96$ μm, $k_{glass} = 1.50$ W m^{-1} K^{-1} [18], $k_{coat} = 0.155$ W m^{-1} K^{-1} [18] and $k_w = 0.605$ W m^{-1} K^{-1} [18] in eqns. 24–27 yields the values $c_{inner} = 0.1315$ K W^{-1}, $c_{glass} = 0.1359$ K W^{-1}, $c_{coat} = 0.0663$ K W^{-1} and $c_{surr} = 4.4972$ K W^{-1}. Each of the four temperature difference terms is tabulated as a percentage of the total temperature difference in Table II. More than 90% of the resistance to heat transfer is in the air film on the outer jacket of the capillary. This means that one should focus on this resistance if the heat removal should be more effective.

Inserting $c_{surr} = 4.4972$ K W^{-1} in eqn. 29 results in a heat-transfer coefficient of 369 W m^{-2} K^{-1} for the air-bath-thermostated capillary in the ABI Model 270A HPCE instrument. In the Beckman P/ACE System 2000 HPCE instrument, where the capillary is thermostated with circulating liquid by the use of a Peltier device, similar calculations gave an h value of 501 W m^{-2} K^{-1} when a 75 μm I.D. capillary was employed for the analysis (50 μm I.D. in the ABI Model 270A). It is surprising that the heat-transfer coefficient is only slightly larger for the liquid cooling than the air cooling.

TABLE II

EACH OF THE FOUR TEMPERATURE GRADIENTS IN EQN. 22 WRITTEN AS THEIR PERCENTAGE OF THE TOTAL TEMPERATURE GRADIENT, dT

The values were obtained by solving eqns. 24–27 with the appropriate experimental values. More than 90% of the total heat flux resistance is in the air film on the outer wall of the capillary tube. Hence this air film acts as a "thermo layer".

dT_X	$\frac{dT_X}{dT} \cdot 100$ (%)
dT_{inner}	2.7
dT_{glass}	2.8
dT_{coat}	1.4
dT_{surr}	93.1
Total	100.0

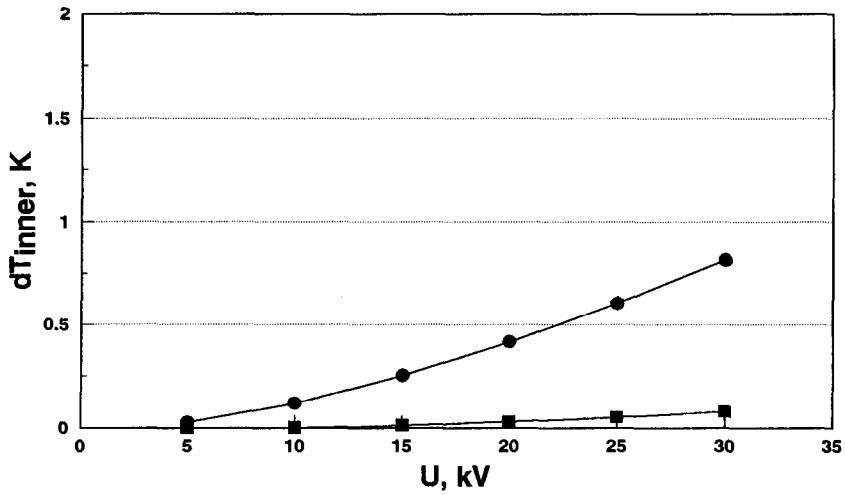

Fig. 10. Sample zone temperature gradient from the capillary tube axis to the inner radius (dT_{inner}, K) *vs.* the applied potential (U, kV) in the (●) stacking and (■) non-stacking runs. Experimental conditions as in Fig. 1.

As only 2.7% of the total temperature difference is from the centre of the capillary tube to the glass wall in the air-bath-thermostated HPCE apparatus (Table II), a dT value of 10°C only results in a dT_{inner} value of 0.27°C. Fig. 10 shows the calculated dT_{inner} values of the sample zone in the stacking and non-stacking experiments. In Fig. 11 the estimated sample zone temperatures when employing the running buffers with three different NaCl concentrations are plotted. The dT_{inner} values are kept within 2°C even at dT_S values of *ca.* 70°C (30 kV, tricine buffer with 50 m*M* NaCl). These results are in accordance with similar calculations reported by Grushka *et al.* [18] and Knox [19].

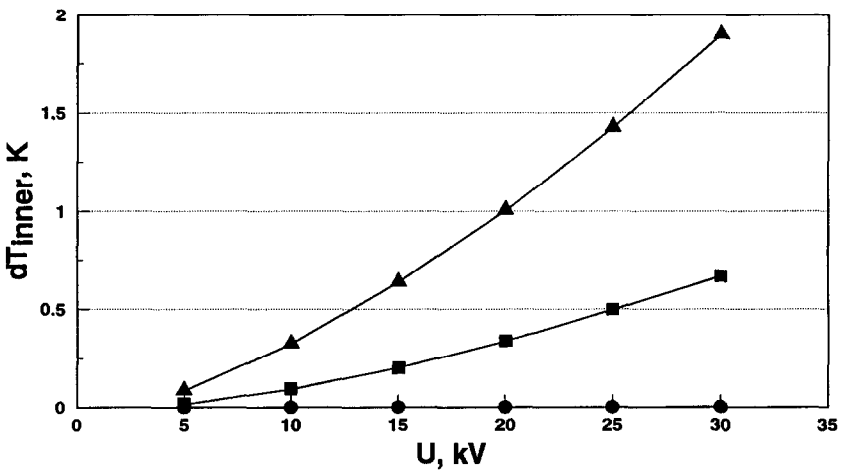

Fig. 11. Sample zone temperature gradient from the capillary tube axis to the inner radius (dT_{inner}, K) *vs.* the applied potential (U, kV) in the three experimental series where the 10 m*M* tricine buffer (pH 8.0) contained (●) 0, (■) 25 or (▲) 50 m*M* NaCl. Experimental conditions as in Fig. 8.

Two approaches can be considered in order to minimize dispersion caused by Joule heating of the analyte zone. Either the heat removal should be very effective, thus minimizing the total temperature gradient, dT, or the dT_{inner}/dT ratio should be kept low. The latter is accomplished either by increasing the surface-to-volume ratio of the capillary tube or by making the glass tube, the polyimide coating and/or the "thermo layer" on the capillary tube act as a heat-transfer resistor, which increases the overall dT, however. A combination of the air film acting as a heat-transfer resistor (by the use of the thermostated air-bath) and a small capillary I.D. and O.D. was used in the actual experiments. While the dT_{inner} to dT percentage ratio for the thermostated air-bath was 2.7%, the corresponding value for the Peltier-based liquid cooling system was 11.7%. When a 75 μm I.D. capillary is used in the Beckman P/ACE System 2000 and a 50 μm I.D. capillary is used in the ABI Model 270A, almost identical temperatures are obtained when identical buffers and field strengths are employed. Hence, with the same temperatures inside the capillaries, the additional analyte zone dispersion caused by Joule heating is largest when liquid cooling is used. The overall dT is, however, lower in the liquid-cooled system when identical I.D. and O.D. capillaries are used in the two instruments.

The relatively low temperature elevations as a function of radial position in the liquid, dT_{inner}, should not be confused with the fact that the buffer/sample zone as a whole experiences an elevated temperature, dT.

REFERENCES

1 B. L. Karger, A. S. Cohen and A. Guttman, *J. Chromatogr.*, 492 (1989) 585.
2 W. G. Kuhr, *Anal. Chem.*, 62 (1990) 403R.
3 C. L. Rice and R. Whitehead, *J. Phys. Chem.*, 69 (1965) 4017.
4 M. Martin, G. Guiochon, Y. Walbroehl and J. W. Jorgenson, *Anal. Chem.*, 57 (1985) 559.
5 A. Vinther and H. Søeberg, *J. Chromatogr.*, 559 (1991) 3.
6 J. W. Jorgenson and K. D. Lukacs, *Science*, 222 (1983) 266.
7 X. Huang, W. F. Coleman and R. N. Zare, *J. Chromatogr.*, 480 (1989) 95.
8 H. H. Lauer and D. McManigill, *Trends Anal. Chem.*, 5 (1986) 11.
9 F. Foret, M. Deml and P. Bocek, *J. Chromatogr.*, 452 (1988) 601.
10 S. Hjertén, *Electrophoresis*, 11 (1990) 665.
11 W. Th. Kok, *Zone Broadening in Capillary Zone Electrophoresis*, Amsterdam Summer Course in Capillary Zone Electrophoresis, University of Amsterdam, Amsterdam, 1990.
12 S. Terabe, K. Otsuka and T. Ando, *Anal. Chem.*, 61 (1989) 251.
13 S. Terabe, paper presented at the *3rd International Symposium on High Performance Capillary Electrophoresis (HPCE '91), San Diego, CA, Feb. 3–6, 1991* paper LW-3.
14 J. H. Knox and K. A. McCormack, *J. Liq. Chromatogr.*, 12 (1989) 2435.
15 K. D. Lukacs and J. W. Jorgenson, *J. High Resolut. Chromatogr. Chromatogr. Commun.*, 8 (1985) 407.
16 S. Terabe, K. Otsuka and T. Ando, *Anal. Chem.*, 57 (1985) 834.
17 A. E. Jones and E. Grushka, *J. Chromatogr.*, 466 (1989) 219.
18 E. Grushka, R. M. McCormick and J. J. Kirkland, *Anal. Chem.*, 61 (1989) 241.
19 J. H. Knox, *Chromatographia*, 26 (1988) 329.
20 R. J. Nelson, A. Paulus, A. S. Cohen, A. Guttman and B. L. Karger *J. Chromatogr.*, 480 (1989) 111.
21 V. P. Burolla, S. L. Pentoney and R. N. Zare, *Am. Biotechnol. Lab.*, Nov./Dec. (1989) 7:10, 12.
22 D. C. Crow, *Principles and Applications of Electrochemistry*, Chapman & Hall, London, 1988.
23 T. S. Stevens and H. J. Cortes, *Anal. Chem.*, 55 (1983) 1365.
24 D. S. Burgi, K. Salomon and R.-L. Chien, presented at the *2nd International Symposium on High Performance Capillary Electrophoresis (HPCE '90), San Francisco, CA, Jan. 29–31, 1990*, poster P-112.
25 R. C. Weast and M. J. Astle (Editors), *CRC Handbook of Chemistry and Physics*, CRC Press, Boca Raton, FL, 62nd ed., 1982, E-51.
26 S. E. Moring, J. C. Colburn, P. D. Grossman and H. H. Lauer, *LC · GC Int.*, 3 (1990) 46.
27 R. B. Bird, W. E. Stewart and E. N. Lightfoot, *Transport Phenomena*, Wiley, New York, 1960.